Fabrication and histological evaluation of calcium carbonate- and carbonate apatite-coated titanium implants

石, 瑞

Fabrication and histological evaluation of calcium carbonate- and carbonate apatite-coated titanium implants

Thesis

Submitted as a partial fulfillment of the requirements

for the degree of Doctor of Philosophy (Dental Science)

Rui Shi

Department of Biomaterials

Graduate School of Dental Science

Kyushu University

Fukuoka, Japan 2020

List of publications and presentations

Publications

R. Shi, K. Hayashi, K. Ishikawa, Rapid osseointegration bestowed by carbonate apatite coating of rough titanium. Advanced Materials Interfaces, submitted.

R. Shi, K. Hayashi, L. Bang, K. Ishikawa, Effects of surface roughening and calcite coating of titanium on cell growth and differentiation. Journal of Biomaterials Applications 34, 917–927 (2019).

R. Shi, Y. Sugiura, K. Tsuru, K. Ishikawa, Fabrication of calcite-coated rough-surface titanium using calcium nitrate. Surface and Coatings Technology 356, 72–79 (2018).

Presentations:

R. Shi, K. Hayashi, K. Ishikawa, Effect of calcite-modified titanium implant surfaces on osseointegration. 第 55 回九大生体材料・力学研究会, 福岡, 2019. 12.

Table of contents

Abstract

Titanium (Ti) implants that realize rapid osseointegration are required for favorable outcome. Rough implant surfaces favor osseointegration, and the coating of implants with natural bone mineral, i.e., carbonate apatite (CO_3Ap), may be effective for osseointegration. To achieve rapid osseointegration, rough Ti substrates were coated with CO_3Ap (CO_3Ap-Ti), and the effects were evaluated in vitro and in vivo. For comparison, rough Ti without coating (rough-Ti) and calcium carbonate-coated rough Ti ($CaCO_3$-Ti) substrates were fabricated. The adhesive strengths of $CaCO_3$ and CO_3Ap to the substrates were ~56.6 and ~76.8 MPa, respectively, being significantly higher than the strength defined in ISO13779-2 (15 MPa). $CaCO_3$ and CO_3Ap coatings significantly promoted pre-osteoblastic MC3T3-E1 cell proliferation. Additionally, the CO_3Ap coating promoted higher osteogenic differentiation activity than $CaCO_3$ coating. CO_3Ap-Ti implantation into rabbit tibia defects prompted bone maturation, compared to $CaCO_3$-Ti or rough-Ti implantation. The bone-implant contact percentage with CO_3Ap-Ti and $CaCO_3$-Ti was higher than that with rough-Ti. Consequently, CO_3Ap-Ti acquired robust bond with the host bone at early stage (four weeks post-implantation), compared to $CaCO_3$-Ti and rough-Ti: the CO_3Ap-Ti–bone bonding strength was ~1.9- and ~5.5-fold higher than that of $CaCO_3$-Ti and rough-Ti, respectively. Thus, CO_3Ap coating of Ti implants was effective for achieving rapid osseointegration.

Chapter 1. Introduction

1.1. Titanium for biomedical applications

Titanium is widely used as implant materials on account of their exceptional biocompatibility, high specific properties in mechanic and chemical, excellent corrosion resistance, and lower elastic modulus than other metals (results in less stress shielding and inhibits bone resorption around the implant), making it suitable for use in the replacement of failed hard tissues and dental applications.[1,2] Intensive researches on implant material revealed that useful orthopedic and dental implants heavily depend on direct structural and functional connection between the living bone and surface of a load-bearing implant, termed osseointegration.[3,4] However, an implant that can be osseointegrated does not always translate into success, especially in the case of the Ti implant without modifications since the bio-inertness oxide layer of Ti has hindered the direct bonding and active stimulation of bone formation around the surface of Ti implants.[5,6]

Although the existing researches revealed that the oxide layer of Ti leads to its corrosion resistance and biocompatibility; the biocompatibility of Ti is related to the capacity of the Ti oxide layer to react with water ions and serum proteins as well as the resistance to corrosion that provided by the oxide layer.[7,8] When implants do not undergo modification, it takes a relatively long time to fix the Ti implant to bone such that it is stable. Insufficient integration can lead to the formation of fibrous tissues and the ensuing loosening of the prostheses.[9,10] Therefore, endless efforts have been made worldwide to investigate ways to improve insufficient osseointegration property.

1.2. Methods to enhance osseointegration properties

The osseointegration properties of Ti implants can be improved in a variety of approaches, mainly including topographical modification and the introduction of surface coating since the surface properties of Ti have a significant influence on osseointegration.[11] The surface properties of bone-implant material are inextricably linked to the adhesion, proliferation, differentiation, and mineralization of osteogenic cells, which in turn affect the generation of new bone tissue around the implant and the long-term stability of the prosthesis.[12-15]

1.2.1. Topographical modification

The preparation of rough material surfaces is the dominant direction of implant surface modification research. Surface nanoscale roughness, which directly corresponds to the sizes of proteins and cell membrane receptors, could also play an important role in osteoblast differentiation and tissue regeneration.[16] The increased roughness of the Ti surface reduces the incidence of soft tissue inventing in the early implant period while enhancing the strength of the implant-osteointegration interface and increasing the implant osseointegration rate.[17] To date, however, the optimum roughness of the implant surface has not been determined. Research in this area has shown that macroscopic roughness (> 10 μm) affects the mechanical properties of the implant interface, the way stress is distributed and delivered, the mechanical locking of the interface; microscopic roughness (10 nm – 10 μm) is close in size to the cellular, biological macromolecular size and affects the biological effects of the implant surface interface; nanoscale roughness (< 10 nm) has important effects on protein adsorption, osteoblast adhesion, and increased

bone binding rate. Compared to smooth Ti surfaces, micron-scale Ti surfaces affect cell adhesion, which in turn improves the histological response after implant placement.[17]

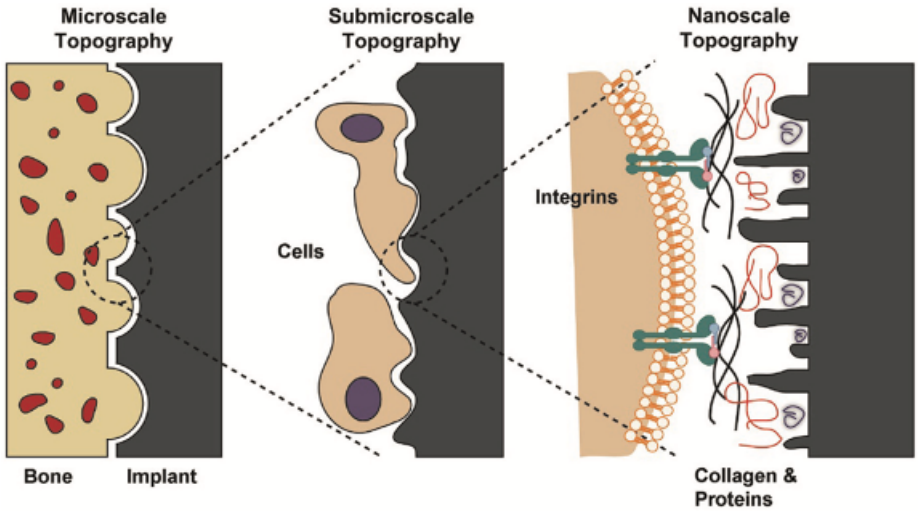

Figure 1. Schematic of the interactions between bone and the implant surface at different topographical scales.[16]

In principle (Figure 1), surface topography can affect the number of cells and platelet that adhere to implant surfaces from blood occurs in seconds.[16,18] Increased clot retention measured at acid-etched implant surfaces that resulted in ingrowth of bone and improved osseointegration.[18,19] In vitro studies state that topographical modification of the surface causes a topographical cue to elicit the cellular signaling pathways for active structural and functional connections between the material-cell interfaces, the attachment of proteins and osteogenic cells, and consequently improve the bone formation directly on the surface and osseointegration.[20] Many attempts have become a research hotspot in recent years to improve the surface properties of existing implants. The surface treatment of commercially pure titanium implants is also carried out by different modification techniques, including mechanical modification (machining, grinding, and blasting),

chemical modification (acid etching, alkali etching, and anodization), promoting the osseointegration ability to achieve the desired implantation result.[21,22]

1.2.2. Surface coating

The surface coating method combines several bioactive materials with the Ti surface. The coating materials confer Ti an excellent osteoconductivity that could accelerate the growth of bone tissue on its surface and promote a strong bond between the implant and surrounding bone.[23,24] That exploits the advantages of Ti and overcome its weaknesses.

The precipitation, nucleation, and growth of the calcium-phosphorus phase are critical physiological processes in the formation of osseointegration in the implant.[25] For now, calcium orthophosphate materials, especially hydroxyapatite [HAp, $Ca_{10}(PO_4)_6(OH)_2$], have been widely employed as the coating materials of Ti owing to their resemblance to the natural bone composition. These coatings are bioactive material with excellent osteoconductivity.[26,27] The introduction of coatings on the surface of Ti can alter the implant surface's physicochemical properties such as roughness, hydrophilicity, surface area, and so on. The coated surface thus facilitates the adsorption and interaction of extracellular matrix proteins, thus promoting the adhesion, proliferation, and differentiation of osteoblasts.[28,29] Animal experiments have shown that HAp coating accelerates implant-to-bone bonding, increases bone formation between the bone-implant interface, and can form a strong bond with bone tissue in a short time.[29,30]

1.3. Hydroxyapatite coating

HAp is a representative bioactive material in calcium phosphate family, and its composition is similar to that of human bone mineral.[31,32] Therefore, HAp coating of Ti

implants have been studied for decades. HAp coatings have been announced to assist early bone formation around implants and promote the attachment and differentiation of mesenchymal cells into osteoblasts on its surface.[33-35] Furthermore, in an animal study, HAp-coated Ti implants showed an increased coronal bone growth that was not observed with control Ti implants.[36] The same results were observed in other animal models that bone adapts in much less time to HAp-coated implants compared to uncoated Ti implants.[37,38] For clinical use, a study has indicated HAp-coated implants to have a higher percentage of bone-to-implant contact within 12 months implantation as opposed to commercially pure Ti screws.[39]

However, the long-term effectiveness of HAp coating has been proposed, creating numerous controversies. Recent studies have revealed poor adhesion and low-resorbability of HAp coating cause delamination upon prostheses and consequently generate osteolysis and aseptic loosening.[40,41] HAp-coated devices have lost favor in part because of the rate and severity of infectious complications.[42] The coated implants' biological effect mainly depends on the coating materials, and strong adhesion to the substrate is a prerequisite for expressing the biological effect of the coatings on the implant surface. Problems such as insufficient bonding strength between the coating and the implant, and differences in solubility between different objects, can lead to the coating peeling off and the release of particles on the implant surface. These problems are associated with a high risk of implant failure. In fact, a long-term clinical study reported that the cumulative success rate of HAp-coated implants decreased to 77.8% after eight years.[43] Another clinical study has also shown that the failure rate of HAp-coated implants

increases significantly after 5 and 10 years.[44] Therefore we should develop a new coating material to overcome the disadvantages of HAp.

1.4. A potential material for coating

Table 1. Hard tissue components of the human adult.[45]

Element	Enamel	Dentine	Bone
Ca^{2+}	36.5	35.1	34.8
PO_4 as P	17.7	16.9	15.2
CO_3^{2-}	3.5	5.6	7.4
Na^+	0.5	0.6	0.9
Mg^{2+}	0.4	1.2	0.7
Cl^-	0.3	< 0.1	0.1
$P_2O_7^{4-}$	< 0.1	< 0.1	< 0.1
K^+	< 0.1	< 0.1	< 0.1
F^-	< 0.1	< 0.1	< 0.1
Total Inorganic	97.0	70.0	65.0
Absorbed H_2O	1.5	10.0	10.0

Human adult bone mineral is mainly composed of Ca, CO_3, and PO_4 ions, although trace elements of less than 1% are contained (Table 1). Thus, the bone mineral composition is carbonate apatite (CO_3Ap) rather than HAp. In the apatitic lattice of CO_3Ap, both the OH site and PO_4 site of HAp are substituted with the CO_3 site.[45] CO_3Ap is reported to have higher osteoconductivity than Hap.[46-48] Furthermore, CO_3Ap can be replaced by bone in coordination with bone remodeling, whereas HAp is poorly resorbed and remains at the implantation site for more than 10 years.[46,49,50] Therefore, the CO_3Ap coating of Ti implants may resolve the above-mentioned problems of HAp coatings As a result, CO_3Ap coating is expected to reduce the risk of exfoliation for long-term implants and be effective for rapid and satisfying osseointegration.

However, CO_3Ap coating of Ti implants cannot be achieved by conventional methods such as spray coating and spin coating because CO_3Ap is decomposed by heat.[51] A high sintering temperature leads directly to more loss of CO_2 from the breakdown of carbonate. In fact, vertebrates fabricate bone that is composed of CO_3Ap in the body. Thus, it should be possible to fabricate CO_3Ap coating by a process other than sintering. Our research group has developed the dissolution-precipitation reactions forming CO_3Ap from calcium carbonate ($CaCO_3$) without sintering.[52] As shown in Equation 1–2, Ca^{2+} and CO_3^{2-} supplied from $CaCO_3$ are precipitated as CO_3Ap utilizing the PO_4^{3-} in the solution, because CO_3Ap is at the most stable phase thermodynamically or exhibits very small solubility at physiological conditions.[53] These continuous dissolution-precipitation reactions result in the compositional transformation of $CaCO_3$ to CO_3Ap. In dissolution-precipitation reactions, the macroscopic structure of the precursor is maintained, since the precipitated CO_3Ap crystals gradually replaced the precursor crystals from the surface to the inside. This reaction provides the possibility to fabricate the CO_3Ap coating of Ti through a suitable coating precursor.

$$\mathrm{CaCO_3} \rightarrow \mathrm{Ca^{2+}} + \mathrm{CO_3^{2-}} \quad (1)$$

$$\mathrm{Ca^{2+}} + \mathrm{PO_4^{3-}} + \mathrm{CO_3^{2-}} \rightarrow \mathrm{Ca_{10-a}(PO_4)_{6-b}(CO_3)_c} \quad (2)$$

1.5. Objectives of this study

The present study succeeded in robust coating of a rough Ti substrate with $CaCO_3$. Exploiting the $CaCO_3$ coating as a precursor for dissolution-precipitation reactions may be favorable for achieving robust CO_3Ap coating of rough Ti. Herein, CO_3Ap-coated rough Ti substrates (CO_3Ap-Ti), with strong adhesive strength between CO_3Ap coating

and Ti surface, were fabricated by dissolution-precipitation reactions of $CaCO_3$-coated rough Ti ($CaCO_3$-Ti). The proliferation and osteoblastic differentiation of pre-osteoblastic cells on CO_3Ap-Ti, $CaCO_3$-Ti, and rough Ti without coating (rough-Ti) were investigated by in vitro experiments. Furthermore, the osseointegration abilities of CO_3Ap-Ti, $CaCO_3$-Ti, and rough-Ti were evaluated in vivo.

Chapter 2. Fabrication and characterization of calcium carbonate- and carbonate apatite-coated titanium

2.1. Introduction

CO_3Ap coating has massive potential as a coating material for rapid osseointegration and long-term survival of Ti implant. In this chapter, we describe the coating of Ti with CO_3Ap by the dissolution-precipitation reactions and the structural and mechanical properties of CO_3Ap coating.

2.2. Material and method

2.2.1. Material

Unless otherwise stated, all chemicals used in this study were purchased from Wako Pure Inc., Co. (Osaka, Japan). Grade II commercial pure Ti (smooth-Ti) was purchased from T&I Co (Saitama, Japan). Two specifications of smooth-Ti, disks and plates, were prepared for in vitro and in vivo evaluations, respectively. The Ti disks were 14.5 mm in diameter and 1 mm in height, and the Ti plates were 10 mm in length and 1 mm in height.

2.2.2. Sample preparation

The sample preparation process is summarized in Figure 2. The smooth-Ti was roughened in a dual-acidic solution of 50 vol% H_2SO_4 and 7 vol% HCl for 30 min at 70 ℃. The etched Ti (rough-Ti) was then removed from the acid solution and washed in an ultrasonic cleaner for 15 min with ethanol and distilled water. The roughening procedure was ended that the samples were allowed to dry at room temperature overnight. Afterward, $Ca(NO_3)_2$ ethanol solution (0.5 M) was prepared as the starting material. The

$Ca(NO_3)_2$ solution (8.25 μL) was added drop-wise to both surfaces of the Ti substrate. When the droplet covered the whole Ti surface, the samples were placed in an electric furnace for heat treatment. The heating program was as follows: the furnace was set to 550 ℃ at a heating rate of 3 ℃ min^{-1}, kept at the constant temperature for five hours, and then cooled in the furnace to room temperature naturally. The process was performed under 100 mL min^{-1} CO_2 gas flow. In addition, the rough-Ti without $Ca(NO_3)_2$ was treated following the above-explained heat protocol to generate control samples.

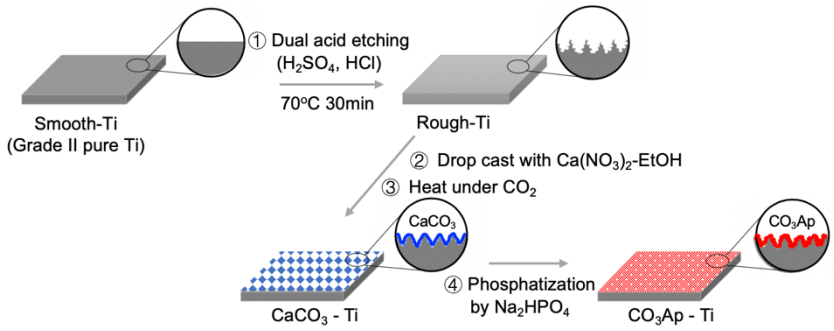

Figure 2. Schematic of the sample preparation and experimental methods.

For composition conversion of the coating from $CaCO_3$ to CO_3Ap, each $CaCO_3$-Ti was soaked in Na_2HPO_4 aqueous solution (30 mL, 0.2 M) at 80 ℃ for seven days. As a result, CO_3Ap-Ti was obtained. The CO_3Ap-Ti was immersed in distilled water (30 mL) at the same temperature for 24 h to remove the residual Na_2HPO_4 solution from the Ti surface. Finally, the CO_3Ap-Ti was rinsed with distilled water three times and dried at room temperature.

2.2.3. Analysis of surface characteristics

The surface and cross-sectional morphologies of the sample were acquired by SEM (S-3400N, Hitachi High-Technologies Co., Tokyo, Japan) after sputter-coating with gold-palladium (MSP-1S, Hitachi, Tokyo, Japan). Besides, the cross-section of samples was also recorded by EDX spectroscopy, which was coupled to SEM. X-ray intensities of calcium (Ca, purple), phosphorus (P, yellow), and titanium (Ti, cyan) were analyzed across the interface to evaluate the thickness of the coating. The coating polymorphism on the Ti surface was identified by an X-ray diffractometer (XRD, D8 Advance, Bruker AXS GmbH, Karlsruhe, Germany) using Cu-Kα radiation generated at 40 kV and 40 mA. The 2θ ranged from 10° to 40° at 2° min^{-1} step using a resolution of 0.02°, where θ is the diffraction angle. The chemical structure of the coating was analyzed by Fourier transform infrared spectroscopy with attenuated total reflection accessories (ATR-FTIR; FT/IR-6200; JASCO Co., Tokyo, Japan); the background spectrum was obtained by scanning the noncoated rough-Ti substrate. Additionally, HAp powders (HAp-200, Taihei Chemical Industrial Co., Osaka, Japan) were analyzed by ATR-FTIR and served as a control. The arithmetic mean deviation surface roughness (Ra) and topography were measured by laser scanning confocal microscopy (LSCM; VK-9710, Keyence, Japan). Contact angles were measured with a contact angle meter (DM500, Kyowa Interface Science, Saitama, Japan); measurements were made after carefully dropping water (1 μL/droplet) onto the material surfaces until 30 seconds (n=8). The adhesive tensile strength of the coating on Ti was determined by the pull-off test, using a universal mechanical strength tester (Romulus, Quad Group Inc., NY, USA). The surface of coated Ti was bound to the stud with prefabricated thermosetting resin (diameter of 2.7 mm).

The stud was then pulled off at a rate of 2 mm sec^{-1}, and the load was recorded until the sample detached from the Ti surface. The maximum load was recorded and converted to pressure as the adhesive strength of the coating.

2.2.4. Statistical analysis

Statistical and graphical analysis was performed using Prism 8.2.1 (GraphPad Software, Inc., La Jolla, CA, USA). The data gathered from each experiment were used to calculate the mean with standard deviation (Mean ± SD). Base on the normal distribution of data and group numbers in each experiment, Student t-test and one-way ANOVA (Fisher's LSD test and Kruskal-Wallis test) were chosen correspondingly to analyze the statistical difference. A probability level of less than 0.05 ($p < 0.05$) was considered a significant difference between the two groups.

2.3. Results

2.3.1. Surface morphologies

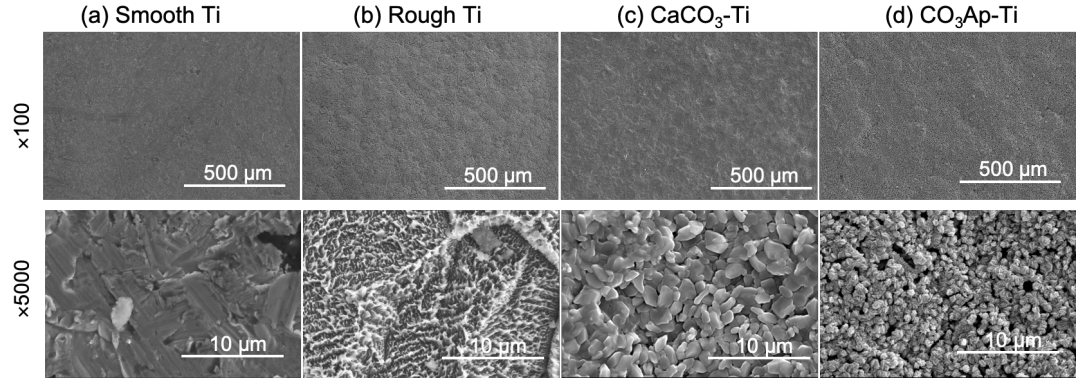

Figure 3. SEM micrograph of smooth-Ti (a), rough-Ti (b), $CaCO_3$-Ti (c), and CO_3Ap-Ti (d). The magnifications of each image are ×100 and ×5000, respectively, from top to bottom in each vertical row.

The surface and interface morphologies of the samples were observed by scanning electron microscopy (SEM). The SEM images (Figure 3) showed that the surface of rough-Ti was rough and uneven with numerous micro-holes, whereas that of $CaCO_3$-Ti was fully coated with cubic or needle-like particles, with a visible aggregation of crystals and no uncoated regions. CO_3Ap-Ti surface was also coated with a uniform layer composed of spherical particles.

2.3.2. Surface topography, roughness, and wettability

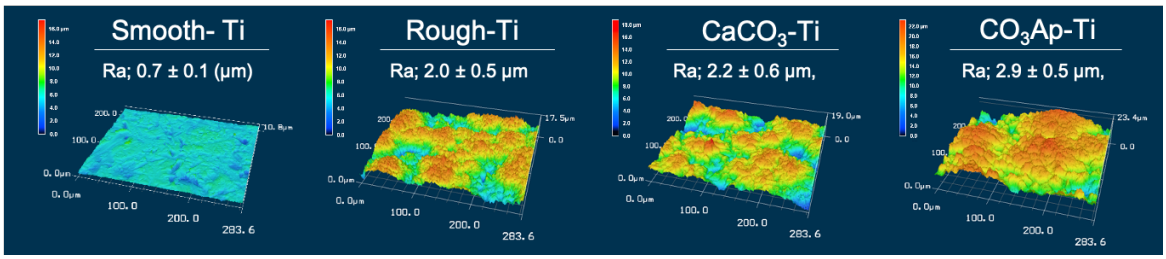

Figure 4. Arithmetic mean roughness (Ra) and 3D laser scanning microscopy images of smooth-Ti, rough-Ti, $CaCO_3$-Ti, and CO_3Ap-Ti. Ra: arithmetical mean deviation of the assessed profile (n = 4).

The surface roughness and topography of the sample surfaces were measured by 3D-laser scanning (Figure 4). The topography and roughness of smooth-Ti increased after acid etching and coating procedures. The 3D profiles captured for evaluation of the topography of each sample revealed that the surface of the CO_3Ap-Ti was vastly different in height (peak-to-valley view) compare to $CaCO_3$-Ti and rough-Ti surfaces. The Ra values for arithmetical mean deviation were calculated as a parameter describing the difference in the roughness of the sample surfaces. The Ra values of CO_3Ap-Ti, $CaCO_3$-Ti, rough-Ti and smooth-Ti were 2.9 ± 0.5 µm, 2.2 ± 0.6 µm, 2.0 ± 0.5 µm and 0.7 ± 0.1 µm, respectively. Thus, A significant increase was observed in surface roughness after

acid etching ($p < 0.05$). The Ra value of CO_3Ap-Ti was significantly higher than that of $CaCO_3$-Ti and rough-Ti ($p < 0.05$), whereas there was no significant difference between $CaCO_3$-Ti and rough-Ti.

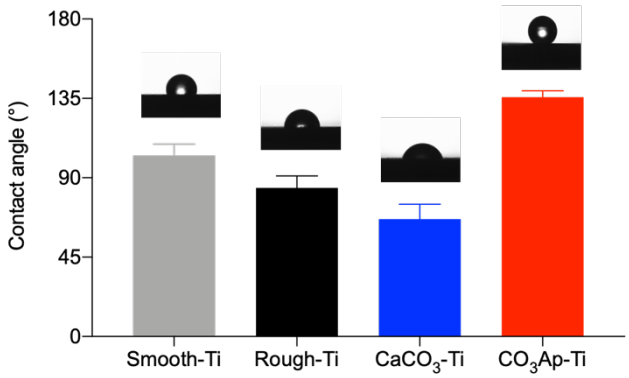

Figure 5. Quantification and optical images of water contact angles on smooth-Ti, rough-Ti, $CaCO_3$-Ti, and CO_3Ap-Ti surfaces ($n = 8$).

The results of contact angle (Figure 5) indicated that acid etching process or $CaCO_3$ coating could significantly decrease the contact angle of the water ($p < 0.05$), in other words, the hydrophilicity of the Ti surface is improved by roughening process and $CaCO_3$ coating. However, CO_3Ap-Ti shows an opposite high contact angle, which means the surface has higher hydrophobicity.

2.3.3. Coating chemical compositions (cross-section view)

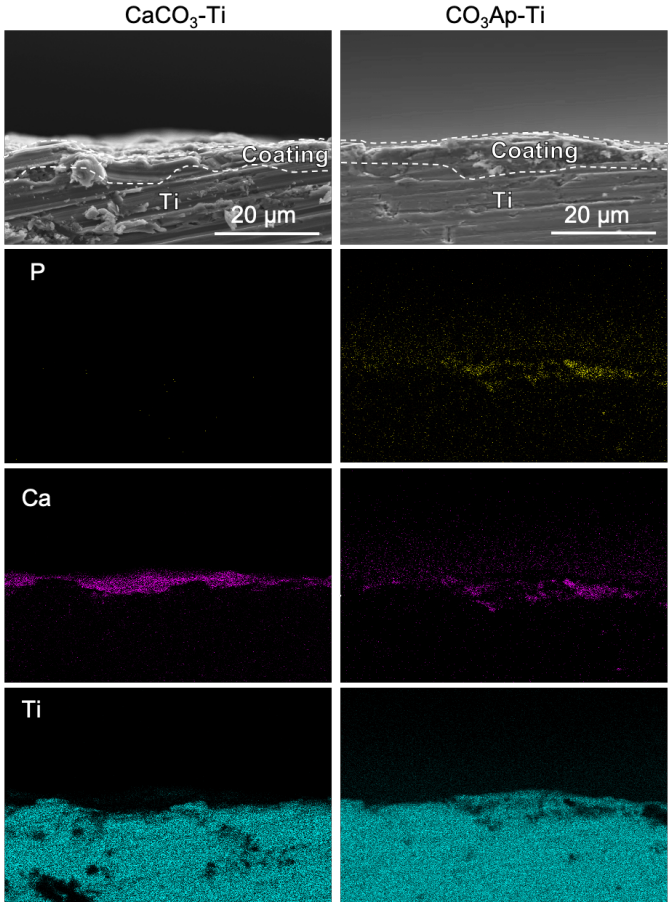

Figure 6. Cross-section SEM and corresponding EDX P, Ca, and Ti maps in $CaCO_3$-Ti and CO_3Ap-Ti (×2000). X-ray intensities of calcium (Ca, purple), phosphorus (P, yellow), and titanium (Ti, cyan).

Cross-section EDX element mapping (Figure 6) showed that both calcium and phosphorus ions were detected on the CO_3Ap-Ti surface, whereas only calcium ions were present on the $CaCO_3$-Ti surface. These results suggested that CO_3Ap-Ti and $CaCO_3$-Ti were coated with apatite and $CaCO_3$, respectively. Furthermore, the thicknesses of $CaCO_3$ coating and CO_3Ap coating were ~5 μm and ~9 μm, respectively.

2.3.4. Surface chemical compositions

The X-ray diffractometry (XRD) pattern showed that the rutile phase of TiO_2 (rutile phase) was formed in Ti surfaces after annealing (Figure 7). In the XRD pattern of $CaCO_3$-Ti, diffraction peaks derived from $CaCO_3$ (calcite phase) as well as Ti and Titania were detected, indicating that $CaCO_3$ coating was formed on that Ti surface by decomposition of $Ca(NO_3)_2$ and subsequent reaction with CO_2 at 550 ℃. In the XRD pattern of the CO_3Ap-Ti, the diffraction peaks of $CaCO_3$ disappeared, and typical apatite peaks appeared.

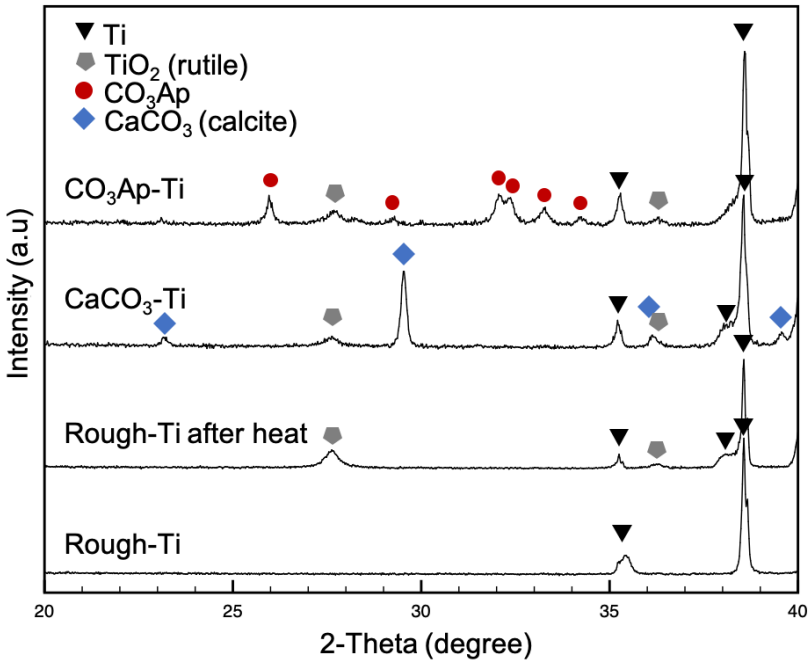

Figure 7. XRD patterns of the surface of rough-Ti, rough-Ti after 550 ℃ annealing, $CaCO_3$-Ti, and CO_3Ap-Ti; the triangles mark the peaks ascribed to the Ti substrate, the pentagon correspond to TiO_2 (rutile), the prisms to the peak of $CaCO_3$ (calcite), and the circle represents the peaks of CO_3Ap.

In the ATR-FTIR spectrum of $CaCO_3$-Ti (Figure 8), carbonated bands were present at 1390 cm^{-1} (ν_3 region), 875 cm^{-1} (ν_2 region), and 720 cm^{-1} (ν_4 region). In the spectrum of HAp, the phosphate bands were observed at 560–600 cm^{-1} and 9601100 $cm^{-1,}$ and the hydroxyl band was observed at 630 cm^{-1}. In the spectrum of CO_3Ap-Ti, the bands assigned to phosphate in apatite were present at 552, 600, 958, and 1010 cm^{-1}, whereas the hydroxyl band was not detected. Furthermore, the spectrum of CO_3Ap-Ti showed carbonate bands at 870 cm^{-1} in 2 region and 1408 and 1458 cm^{-1} in ν_3 region. The doublet carbonate bands at 630 cm^{-1} and 900–1200 cm^{-1} in the ν_3 region indicated that carbonate substituted hydroxyl and phosphate, respectively, in the apatite crystal.

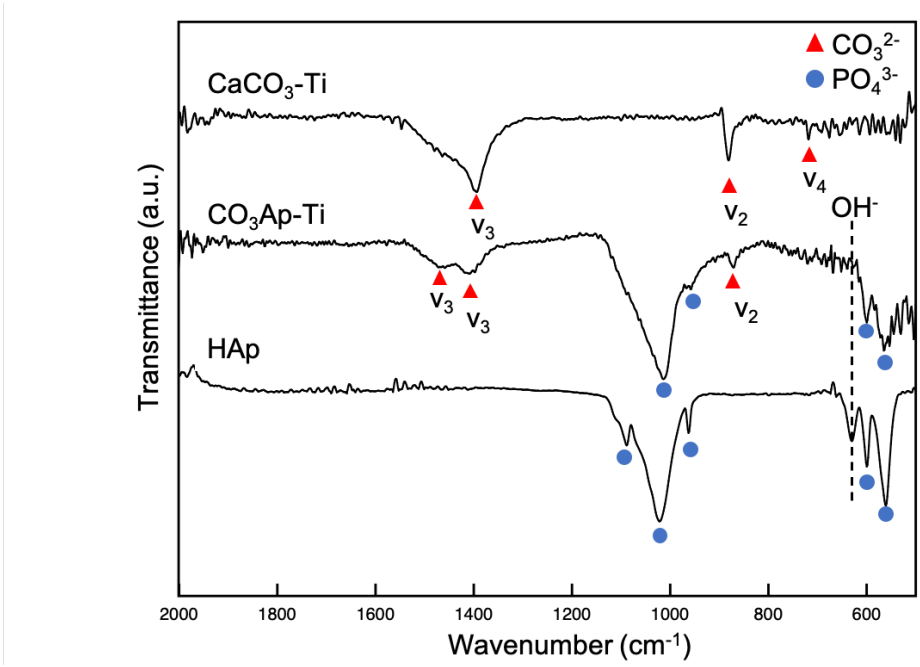

Figure 8. ATR-FTIR spectra of $CaCO_3$ coating, CO_3Ap coating, and HAp powder in the range of 500–2000 cm^{-1}. Red triangles correspond to carbonate bands (1455, 1410, 875, and 720 cm^{-1}), and blue circles mark phosphate bands (960–1100 cm^{-1} and 560–600 cm^{-1}).

2.3.5. Coating adhesive strength to the substrates

The adhesion strengths between coatings and Ti substrates in CO_3Ap-Ti and $CaCO_3$-Ti were measured by the pull-off test. The photographs of the sample surface after the pull-off test (Figure 9a) revealed that both CO_3Ap-Ti and $CaCO_3$-Ti showed a primary adhesion failure mode, as illustrated in Figure 9b, ensuring that the value of the adhesive strength between the coating and Ti substrate was accurately measured. The coating adhesive strengths of CO_3ApTi and $CaCO_3$-Ti were 76.8 ± 2.7 MPa and 56.6 ± 16.1 MPa, respectively (Figure 9c), and the strength of CO_3Ap coating was significantly higher than that of $CaCO_3$ ($p < 0.05$).

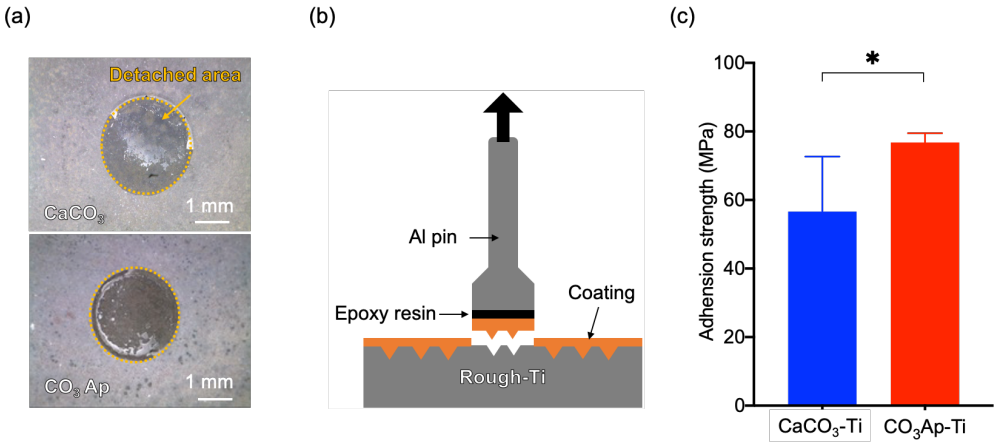

Figure 9. Coating adhesive strength by a standardized pull-off test. (a) Optical photographs revealing the detached area on the $CaCO_3$-Ti and CO_3Ap-Ti surfaces. (b) Illustration of detaching during the pull-off test. (c) Adhesion strength of the coatings. (n = 4) *$p < 0.05$ for comparisons between the indicated groups.

2.4. Discussion

In the present study, we demonstrated the feasibility of the fabrication for $CaCO_3$ and CO_3Ap coatings onto the surface of rough-Ti. The rough-Ti was chosen as the substrate because the adhesive strength of the coating might be improved by taking into account the expanded $CaCO_3$ crystals during heat carbonation process that could interlock with the rough-Ti substrate's micro-scale structures. Besides, as a surface modification method, acid etching could change the wettability, roughness, and surface chemistry of the Ti surface for better biological response.

The XRD, ATR-FTIR results (Figure 7 and Figure 8) demonstrated that Ti substrates were coated with $CaCO_3$, and then the $CaCO_3$ coating was successfully converted into AB-type CO_3Ap.[54,55] First of all, $CaCO_3$ coating of rough-Ti was achieved via thermal decomposition of $Ca(NO_3)_2$ to form CaO and followed by a carbonation reaction of CaO with CO_2 to form $CaCO_3$. The basic concept of this coating technique is the induction of thermal decomposition of $Ca(NO_3)_2 \cdot 4H_2O$ in a CO_2 gas environment. It is known that when $Ca(NO_3)_2 \cdot 4H_2O$ is heated above ~500 °C,[56] it decomposes to CaO, as shown in Equation 3:

$$2Ca(NO_3)_2 \cdot 4H_2O \rightarrow 2CaO + 4NO_2 + O_2 + 8H_2O \quad (3)$$

Resulting CaO can react with surrounding CO_2 so that $CaCO_3$ is deposited on the substrate, as shown in Equation 4:

$$CaO + CO_2 \rightarrow CaCO_3 \quad (4)$$

The above reactions enable the induction of the carbonation reaction below the α–β Ti transition temperature (~880 °C), not causing degradation of the Ti mechanical strength.[57] Therefore, $CaCO_3$ can be coated onto Ti by the heat treatment using a $Ca(NO_3)_2 \cdot 4H_2O$ solution. It is foreseeable that adjusting the concentration or amount of the starting material may optimize the $CaCO_3$ coating amount of the Ti substrate, which changes surface properties of Ti. The type of CO_3Ap was determined by considering where the CO_3 site occupied two different positions in the apatite structure.[46,55] In the present study, the CO_3Ap coating is AB-type, in which both OH and PO_4 sites in apatite lattice were substituted by the CO_3 site. The above analysis of XRD and ATR-FTIR indicates that the purity of both coatings is quite high, and the phosphatization process is fast and thorough under the conditions of this experiment.

The laser microscopy images showed that the rough-Ti has complex topography and roughness compare to smooth-Ti, and the $CaCO_3$-Ti had a similar surface roughness and topography as rough-Ti. Thus, $CaCO_3$ coating was achieved while maintaining the surface roughness and topography of rough-Ti. Afterward, the Ra value of CO_3Ap-Ti was revealed significantly higher than that of $CaCO_3$-Ti, rough-Ti, and smooth-Ti ($p < 0.05$). The addition of $CaCO_3$ and CO_3Ap coatings led to changes in the contact angle of the Ti surface. Presents measurements have not yet confirmed the reason for difference since contact angles are influenced by many factors such as surface energy, surface roughness, surface chemistry, and surface phases.[58] However, recently hydrophobic and superhydrophobic surfaces with anti-corrosion properties have received significant attention from their critical industrial applications.[59]

The coated implants' biological effect depends mainly on the coating materials, and the strong adhesion to the substrate is a prerequisite for expressing the biological effect of the coatings on the implant surface. The results demonstrate that the CO_3Ap coating could coat roughened Ti with adequate adhesive strength. According to the International Organization for Standardization (ISO) 13779-2 Part 2, the tensile coating adhesion of implants for surgery shall be not less than 15MPa (individual >10MPa). The adhesion strength of our CO_3Ap-Ti (76.8±2.7 MPa) was much higher than the ISO requirement even more than the $CaCO_3$'s adhesive strength. The coating strength in $CaCO_3$-Ti was 56.6±16.1MPa, which is significantly higher than that between the coating and substrate in HAp- and other bioactive material-coated Ti substrates, ranging from 10 to 40 MPa.[60-62] This result confirms the association between particle size and substrate that the micron-size particle could improve the mechanical strength by interlocking to the rough surface of the substrate. This improved adhesive strength makes CO_3Ap-coated Ti proper for clinical applications.

2.5. Conclusion

In conclusion, a $CaCO_3$ coating layer was successfully prepared on a Ti substrate using a $Ca(NO_3)_2 \cdot 4H_2O$ ethanolic solution as a Ca source. Subsequently, the $CaCO_3$ coating completely converted to CO_3Ap with no residues. The roughening surface remains or even higher after coating procedures; the pull-off test shows that the coatings have sufficient coating adhesive strength on the Ti substrate indicating robust coatings of Ti substrates with $CaCO_3$ and CO_3Ap are achieved.

Chapter 3. In vitro evaluations of calcium carbonate- and carbonate apatite-coated titanium with pre-osteoblastic cells

3.1. Introduction

The adhesion, proliferation, and differentiation of osteoblasts on the implant surface are vital points to osseointegration establishment. In addition to roughness, the surface chemistry and nano-topography of the material modified by surface modification techniques such as mechanical, chemical, and coating could significantly influence on cell differentiation, osteogenesis, and osseointegration.[63-65] Consequently, a cell model has a strong need to identify those effects of coating materials on cellular behaviors, especially for the cell related to osteogenic. MC3T3-E1 cell line, a mouse pre-osteoclast derived from the parietal bone of newborn mice, can differentiate into osteoblasts and form calcified bone nodules in vitro,[66] showing high differentiation and mineralization potential under the combined induction of ascorbic acid and sodium β-glycerophosphate.[67,68]

In the Chapter 2, $CaCO_3$ and CO_3Ap coatings of Ti were successfully fabricated. This chapter describes 1) the differences in the adhesion, proliferation, and differentiation functions of MC3T3-E1 cells on the surface of rough-Ti, $CaCO_3$-Ti, and CO_3Ap-Ti. and 2) the mechanisms of adhesion and functional differentiation of pre-osteoblastic cells on coated-Ti surfaces.

3.2. Material and method

3.2.1. Material

Base on fabrication in the preceding part, rough-Ti, $CaCO_3$-Ti, and CO_3Ap-Ti disks, 14.5 mm in diameter and 1 mm in height, were used as specimens in cell experiments after dry heat-sterilized at 170 °C for one hour. The mouse pre-osteoblastic cell line MC3T3-E1 was obtained from Cell Bank (Riken BioSource, Saitama, Japan).

3.2.2. Cell culture

The cells were cultured in growth medium consisting of alpha-minimal essential medium (α-MEM) supplemented with 10% fetal bovine serum (FBS), penicillin (100 U mL^{-1}), streptomycin (100 μm mL^{-1}), and amphotericin B (0.25 μg mL^{-1}; Thermo Fisher K.K., Tokyo, Japan). The cells were cultured at 37 °C in a humidified air atmosphere containing 5% CO_2. The growth medium was replaced every three days until the cells approached confluence. Then, the confluent cells were harvested using 0.25% trypsin-EDTA solution (Gibco, Thermo Fisher K.K., Grand Island, NY, USA), and seeded into new culture dishes after centrifugation. The above operations are repeated until sufficient amounts of cells were obtained for each test.

3.2.3. Cell attachment

The overall condition of MC3T3-E1 cells attached to the surface of Ti was observed by SEM after a 12-hour culturing period. In brief, MC3T3-E1 cells were seeded on each Ti sample for observation of attachment (as mentioned above) in 24-well plates at 1×10^4 cells $well^{-1}$ (n = 4). The growth medium was aspirated from each well, and cells were washed twice with phosphate-buffered saline (PBS). The washed cells were then fixed

with 1 mL of 3% glutaraldehyde in sodium phosphate buffer at 4 °C for 30 min. Subsequently, the cells were dehydrated in a graded series of ethanol from 50% to 99.5% and evaporated using hexamethyldisilazane. Before SEM observation, the Ti samples with fixed cells were sputter-coated with gold-palladium.

3.2.4. Cell proliferation

MC3T3-E1 cells were cultured at a density of 2×10^4 cells well^{-1} (n = 4) under the conditions explained above for proliferation assessment. The culture medium was changed every two days. At 1, 3, and 7 days, the proliferation of cells was determined using cell counting kit-8 (CCK-8; Dojindo, Kumamoto, Japan). After washing with PBS three times, the samples were incubated in growth medium supplemented with CCK-8 solution at 37 ℃ for 1 h, and 100 μL of the resulting medium was then transferred to a 96-well plate. The absorbance was measured at 450 nm with a microplate reader (M200; TECAN, Victoria, Australia).

3.2.5. Alkaline phosphatase activity

To examine the alkaline phosphatase (ALP) activity, MC3T3-E1 cells were seeded in 24-well plates at an initial density of 6×10^4 cells well^{-1} (n = 4). The cells were cultured in the differentiation medium prepared by supplementing the growth medium with β-glycerol phosphate (10 mM) and ascorbic acid (50 μg mL^{-1}). The culture medium was changed every two days. After 7 and 14 days, the cells were washed in PBS three times and lysed using cell lysis buffer M, and the ALP activity was then assessed using a LabAssay ALP kit. The relative ALP activity is normalized against the total protein

concentration of each sample, which was determined using the Protein Assay Rapid Kit. The activity of each group is expressed, as shown in the calculation below:

$$\text{Relative ALP activity } (\text{nmol/min/}\mu\text{g protein}) = \frac{\text{ALP}(\mu\text{mol/L})}{\text{Protein } (\mu\text{g/L})} \times \frac{1}{\text{ALP incubation time (min)}}$$

3.2.6. Statistical analysis

Statistical and graphical analysis was performed using Prism 8.2.1 (GraphPad Software, Inc., La Jolla, CA, USA). The data gathered from each experiment were used to calculate the mean with standard deviation. Base on the normal distribution of data in each experiment, one-way ANOVA (Fisher's LSD test and Kruskal-Wallis test) was chosen correspondingly to analyze the statistical difference. A probability level of less than 0.05 ($p < 0.05$) was considered a significant difference between the two groups.

3.3. Results

3.3.1. Cell attachments

To evaluate the effects of the coatings of Ti on cell behavior, MC3T3-E1 cells were incubated on CO_3Ap-Ti, $CaCO_3$-Ti, and rough-Ti for 12 h. After 12 h of culture, the MC3T3-E1 cells adhered to the surface of all samples and showed the multilateral spindle shape with pseudopodia (Figure 10).

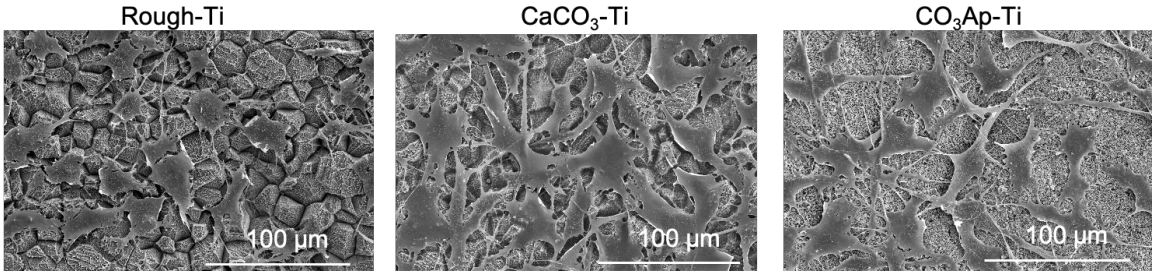

Figure 10. SEM micrographs revealing the morphology of MC3T3E1 cells on the surface of rough-Ti, $CaCO_3$-Ti, and CO_3Ap-Ti at 12 hours after seeding (magnification ×500).

3.3.2. Cell proliferation and differentiation

To further confirm whether the coatings affect the growth of MC3T3-E1 cells, the number of cells on each group was examined by a cell proliferation assay (Figure 11a). On the first day, no significant differences were found between the three groups in MC3T3-E1 cell proliferation. At three and seven days, however, the number of cells on $CaCO_3$-Ti and CO_3Ap-Ti was significantly higher than that on rough-Ti ($p < 0.05$).

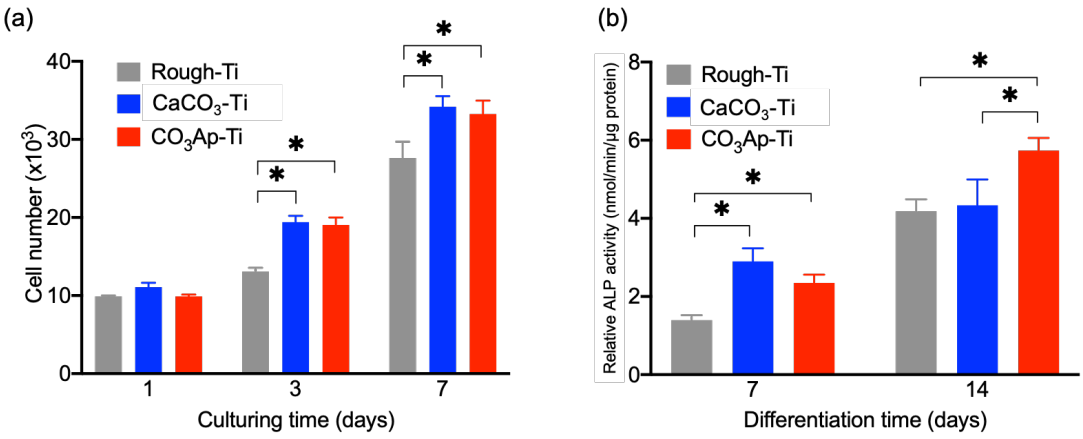

Figure 11. (a) Cell number determined by the cell counting kit-8 (CCK-8) proliferation assay at 1, 3, and 7 days (n = 4); (b) relative ALP activity after 7 and 14 days of incubation (n = 4). *$p < 0.05$ for comparisons between the indicated groups.

Furthermore, relative ALP activity in the $CaCO_3$-Ti and CO_3Ap-Ti groups was significantly higher than that in the rough-Ti group (Figure 11b) at seven days. At 14 days, the ALP activity in the CO_3Ap-Ti group was significantly higher than that in the $CaCO_3$-Ti and rough-Ti groups, whereas no significant difference was observed between the rough-Ti and $CaCO_3$-Ti groups.

3.4. Discussion

The biological response of implant in living bone related to many factors, including chemical, physical, biological, and morphological factors. In order to improve the bioactivity of Ti implants, we gave Ti a bionic coating with rough topography to enhance its biological performance. The appropriate increase in surface roughness of the Ti implant was reported to be conducive to both cell movement and cell growth.[69-71] In addition, Wennerberg et al.[72] suggested that a Ra of ~2 μm in a Ti-based implant surface could provide an optimal degree of roughness to promote osseointegration. These

findings suggested that the Ra values of CO_3Ap-Ti, $CaCO_3$-Ti, and rough-Ti were favorable for reaching potential bone cell differentiation and osseointegration.

The results of the in vitro study demonstrated that CO_3Ap-Ti promotes cell proliferation after three days and differentiation after seven days compared to $CaCO_3$-Ti, followed by rough-Ti. The peak levels of cell anchored and proliferation in $CaCO_3$-Ti was found at the first culturing day. This finding may relate to the solubility of coating ($CaCO_3$ > CO_3Ap in body fluid) that $CaCO_3$-Ti can provide more calcium ions to peri-implant immediately for cell attachment and proliferation since calcium ions are second messengers who regulate gene transcription, cell proliferation, differentiation, and apoptosis.[73] Nevertheless, CO_3Ap-Ti then followed up $CaCO_3$-Ti and significantly improved the ALP activity of MC3T3-E1 cells at 14 days ($p< 0.05$). ALP, the early markers of osteoblast differentiation, has vital implications for bone mineralization. The exciting finding of ALP points out that CO_3Ap-Ti had the potential to boost the differentiation of osteoblastic cells by increasing ALP expression. In summary of in-vitro studies, both $CaCO_3$ and CO_3Ap coated Ti implant can significantly enhance the proliferation and differentiation of MC3T3-E1 cells compare to rough-Ti, and CO_3Ap has high potential to promote the differentiation after seven days. The ALP activity increases observed at seven days in the CO_3ApTi and $CaCO_3$-Ti groups might be attributed to calcium ions released from these coatings because, as reported previously. However, the difference in ALP activity at 14 days between CO_3Ap-Ti and $CaCO_3$-Ti probably corresponded that a proportionate amount of calcium and phosphorus ions released from CO_3Ap.[48,74,75] Thus, CO_3Ap coating is expected to be effective for rapid osseointegration by promoted osteogenic differentiation.

3.5. Conclusion

The CO_3Ap-Ti improved proliferation of pre-osteoblastic cells and promoted their differentiation lastingly toward the osteoblastic phenotype, compared to rough-Ti and $CaCO_3$-Ti. The $CaCO_3$-Ti showed rapid initial adhesion and cell proliferation. However, the promotion of osteoblastic differentiation is short in duration, lasting about seven days while CO_3Ap-Ti effectiveness lasting till 14 days.

Chapter 4. In vivo evaluations of calcium carbonate- and carbonate apatite-coated titanium

4.1. Introduction

The early establishment of osseointegration is conducive to increased postoperative success; conversely, the longer the healing cycle, the higher the risk of implant failure.[76] In the Chapter 3, we demonstrated the positive effect of $CaCO_3$ and CO_3Ap coatings on cellular activity, including proliferation and osteogenic differentiation of pre-osteoblastic cells. This chapter describes the coating effects of Ti implant on initial osseointegration evaluated by histological analyses and mechanical strength measurement.

4.2. Material and method

4.2.1. Materials

Base on fabrication in the preceding part, rough-Ti, $CaCO_3$-Ti, and CO_3Ap-Ti plates, 10 mm in length and 1 mm in height, were used as specimens in animal experiments after dry heat-sterilized at 170 °C for one hour. Adult male Japanese white rabbits (JW/CSK, SLC Inc., Hamamatsu, Japan), aged 19–20 weeks and weighing between 2.9 and 3.1 kg, were used in this study. The animals were housed and cared in the official animal center at Kyushu University and fed standard diet and water ad libitum.

4.2.2. Surgical procedure

To evaluate early osseointegration, CO_3Ap-Ti, $CaCO_3$-Ti, and rough-Ti were implanted into rabbit tibia defects. Animal experiments were conducted following the protocols approved (Approval ID: A19-144-0) by the Animal Care and Use Committee

of Kyushu University. For surgery, the rabbits were anesthetized with an intramuscular injection of ketamine (30 mg kg^{-1}) and xylazine (5 mg kg^{-1}). After shaving and disinfecting with iodine, the proximal tibia was exposed. A hole (1.6 mm in diameter) was made 2 cm away from the knee joint using a straight drill (φ1.6mm, K-501, HOZAN TOOL Inc., Osaka, Japan), and then a straight defect (1.6 mm × 10 mm) was created by sawing straightly from that hole with a diamond file (φ1.6mm, SB-178D, TAIYO SEIKO Inc., Osaka, Japan) under saline rinsing. Ti implants were placed into the defects without extra force, and the incisions were closed with silk sutures. Four weeks later, the rabbits were euthanized by an overdose of anesthesia, and the epiphyses of the tibia block with implant were harvested. An overview of the surgical protocol is shown in Figure 12.

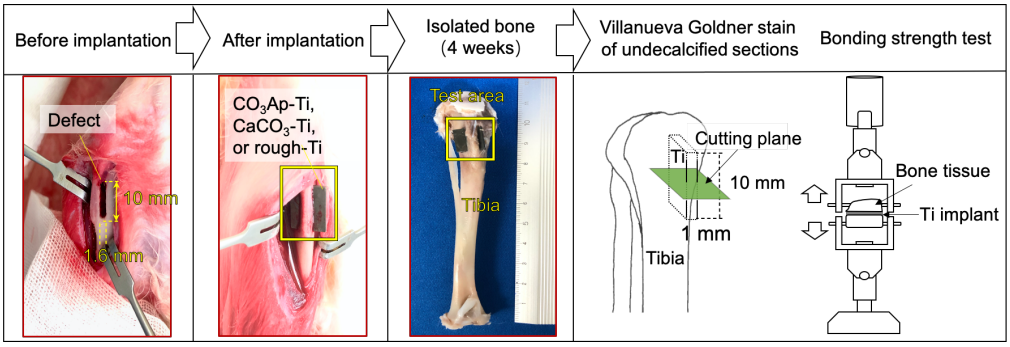

Figure 12. Surgical photographs of the defect created in the tibia (10 mm in length × 1.6 mm in width), the bone harvested at four weeks post-implantation, the illustration of the sectioning and staining method (Villanueva Goldner stain) and bonding strength test.

4.2.3. Bone bonding test and osseointegration observation

Bone was fixed in 10% formalin and dehydrated in a graded alcohol solution, and then embedded in methylmethacrylate (MMA). The embedded tissue was then sectioned into 1-mm-thick slices and ground to the final thickness of 50 μm. In order to quantify

the osseointegration around the Ti implant, the sections were subjected to Villanueva Goldner staining and observed under a microscope (BZX710, Keyence, Osaka, Japan), and the obtained photographs were analyzed to calculate the bone-to-implant contact (BIC). BIC is defined as direct contact between bone and implant without fibrous tissue; The length of new bone touched implants and the implant's total length in the parts that contained compact bone, were measured using image-measurement software (n = 12), and BIC values were determined, as shown in Figure 13.

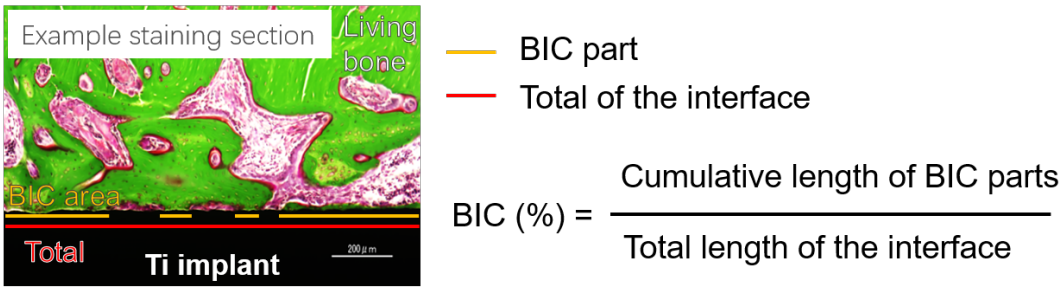

Figure 13. Method of measuring the bone-to-implant contact (BIC) value around implants at parts that contained compact bone.

The harvested bone block with Ti was carefully trimmed to isolate the bone tissue on both sides and at the edges of the plate. A load test device (Figure 12) was set to apply alterable traction to the bone. The detaching failure load was recorded when the implant separated from the bone (n = 8). After testing, the surface of implants was studied using SEM.

4.3. Results

4.3.1. Histological observation and quantification of bone-to-implant contact

At four weeks after implantation, the bone-implant contact (BIC) percentages, an index of osseointegration, were histologically determined by the Villanueva Goldner staining of tissue sections prepared, as shown in Figure 14. The Villanueva Goldner staining stained mineralized bone (MB) green and osteoid pink (Figure 14).

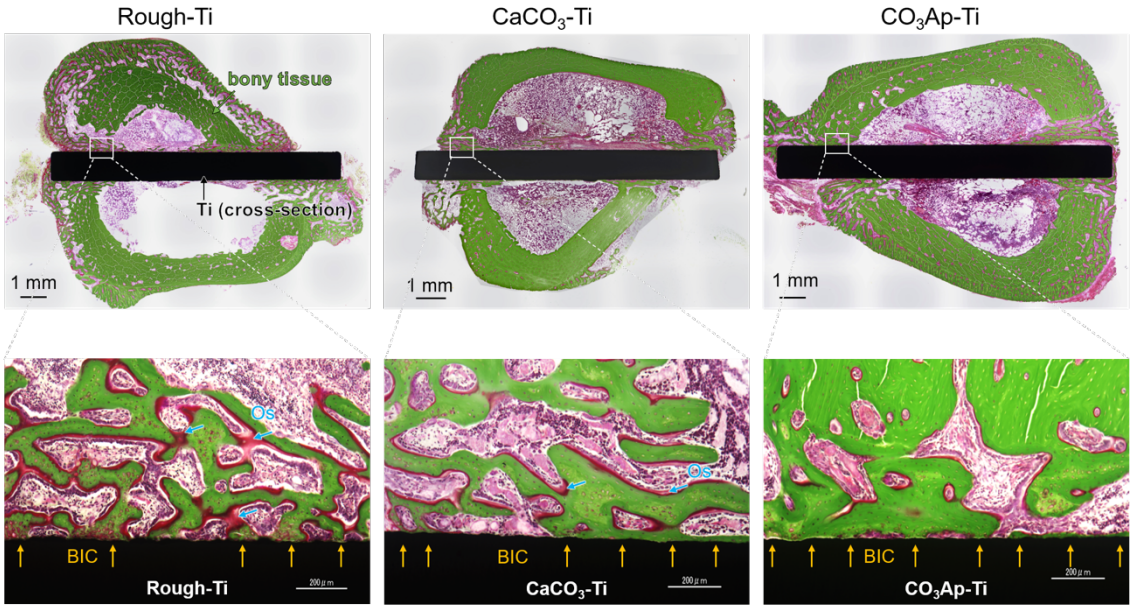

Figure 14. Representative Villanueva Goldner stained histological sections: (up) general view of a representative histological section and (down) high-magnification view of the cortical bone of sections in rough-Ti, $CaCO_3$-Ti, and CO_3Ap-Ti after four weeks of healing showing bone-to-implant contact (BIC) and osteoid (Os). Yellow arrows indicate BIC areas. Cyan arrows highlight unmineralized bone areas.

The histological images at the interface between the implant (i.e., CO_3Ap-Ti, $CaCO_3$-Ti, or rough-Ti) revealed that abundant MB was formed on the CO_3Ap-Ti surface,

whereas osteoid rather than MB was mainly present on the rough-Ti surface (Figure 14). The BIC percentages in rough-Ti, $CaCO_3$-Ti, and CO_3Ap-Ti were 48.2% ± 7.8%, 59.9% ± 15.4%, and 72.9% ± 6.4%, respectively (Figure 15a). Thus, the BIC in CO_3Ap-Ti was significantly higher than that in rough-Ti and $CaCO_3$-Ti.

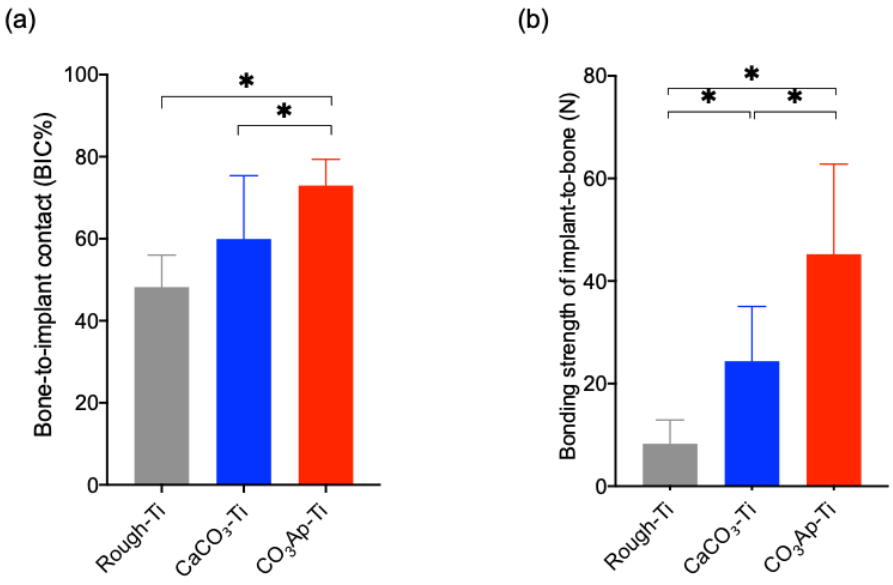

Figure 15. (a) Histomorphometry analysis of newly regenerated bone at four weeks after implantation: BIC in rough-Ti, $CaCO_3$-Ti, and CO_3Ap-Ti (n = 12). (b) The bonding strength of bone-to-implant in rough-Ti, $CaCO_3$-Ti, and CO_3Ap-Ti (n = 8). *$p < 0.05$ for comparisons between the indicated groups.

4.3.2. Bonding strength of the bone-to-implant

Furthermore, the bonding strength between the implant and living bone was evaluated as another index of osseointegration by the detaching test (Figure 15b). The bonding strengths of rough-Ti, $CaCO_3$-Ti and CO_3Ap-Ti to bone were 8.7 ± 4.3 N, 24.0 ± 8.9 N, and 42.5 ± 14.7 N, respectively (Figure 15b). Notably, abundant bone tissue was

observed on the CO_3Ap-Ti surface (Figure 16c), compared to rough-Ti and $CaCO_3$-Ti surfaces (Figure 16a, b).

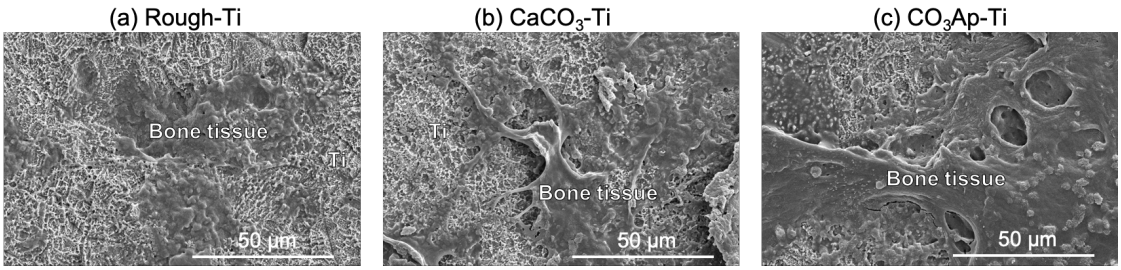

Figure 16. SEM images of the surface of rough-Ti (a), $CaCO_3$-Ti (b), and CO_3Ap-Ti (c) at four weeks after implantation in the tibia defects of rabbits (magnification ×1000).

4.4. Discussion

To evaluate early osseointegration, CO_3Ap-Ti, $CaCO_3$-Ti, and rough-Ti were implanted into rabbit tibia defects for four weeks, and yet the coatings showed stable adhesive behavior during the surgery of implantation. Histological images (figure 14) revealed that abundant mature bone (MB) with less osteoid was formed on the CO_3Ap-Ti surface, followed by $CaCO_3$, whereas osteoid rather than MB was mainly present on the rough-Ti surface. This evidence indicated that the Ti implant with CO_3Ap coating and $CaCO_3$ coating could promote osteogenesis and accelerated maturation of bone matrix. The quantified result shown in figure 15a revealed that BIC was significant improvements in CO_3Ap-Ti ($p > 0.05$). BIC is a term that refers to how much of the implant surface is touching bone. When osseointegration occurs, the percentage of BIC increases, and therefore the stability of the implant in defect increases, which has been reflected in the detaching test (figure 15b). The bonding strengths of rough-Ti, $CaCO_3$-Ti and CO_3Ap-Ti to bone were 8.7 ± 4.3 N, 24.0 ± 8.9 N, and 42.5 ± 14.7 N, respectively (Figure 15b).

Thus, high bonding strength of CO_3Ap-Ti was in agreement with its high BIC. The SEM images of sample surfaces after four weeks post-implantation (Figure 16) showed that the abundant bone tissue was observed on the CO_3Ap-Ti surface, compared to rough-Ti and $CaCO_3$-Ti surfaces. Importantly, a portion of CO_3Ap coating remained (Figure 16c), whereas the $CaCO_3$ coating wholly disappeared (Figure 16b). These differences in resorption speed were derived from the fact that CO_3Ap was mainly resorbed by osteoclastic resorption, and $CaCO_3$ was spontaneously dissolved. Based on the previous in vitro and the present in vivo results, the exceedingly rapid loss of $CaCO_3$ coating caused only extremely short-term positive effects on cell proliferation and differentiation within a week; these positive effects were lost within two weeks. In contrast, the gradual resorption of CO_3Ap coating produced improvements in cell proliferation and differentiation for a more extended period. Even within a week, the effects of CO_3Ap coating were nearly equal to those of $CaCO_3$ coating, according to in vitro results. Therefore, the resorption speed of CO_3Ap coating was considered suitable within four weeks. Compared to the other coating, the adequate resorption speed of CO_3Ap led to superior osseointegration and subsequent replacement of the coating by bone in coordination with bone remodeling, resulting in high BIC and high bonding strength to the living bone.

4.5. Conclusion

The findings clearly indicate that the BIC and bonding strength to the living bone achieved with CO_3Ap-Ti was significantly higher than those with rough-Ti and $CaCO_3$-Ti. Thus, CO_3Ap coating of the Ti implant is more effective for achieving rapid and high-quality osseointegration at the early stage, which seems to be a promising implant

application (e.g., implant fixture or where contact the hard tissue). Further research regarding the long-term efficiency in vivo of this coating material would be worthwhile.

General summary

Surface coatings applied on Ti implants are capable of enhancing osseointegration to limit bone resorption or osteolysis due to inflammation caused by the physiological rejection of materials. Two types of surface coatings applied on roughened Ti substrates, $CaCO_3$ and CO_3Ap, respectively, were investigated. Uniform and thin $CaCO_3$ coating were achieved using a simple drop-cast method. The novel coating features the conversion of $CaCO_3$ to CO_3Ap in more sophisticated morphology; it can be achieved using the dissolution-precipitation reaction technique, which has a great potential in coating complex implant shapes and geometries that are suitable for use in bone and dental applications.

The biocompatibility and cell-implant interaction were investigated using MC3T3-E1 pre-osteoblastic cells. CO_3Ap coating demonstrated overall positive cytoviability with excellent interface interaction (attachment, proliferation, and osteogenetic differentiation). In contrast, the $CaCO_3$ coating has raised a short-term effect and possible rapid dissolution during cell culture that hinders the bioefficacy of the coatings.

Osseointegration was quantified by assessing the bonding strength of mechanical detaching and evaluating bone-to-implant contact (BIC) percentages through the histological stain of the implant perimeter using a rabbit model in four weeks. The BIC and bonding strength to the living bone achieved with CO_3Ap-Ti was significantly higher than those with rough-Ti and $CaCO_3$-Ti. The animal experiment has found that CO_3Ap and $CaCO_3$ coatings can stimulate osteogenic differentiation, bone mineralization, and osseointegration processes with different efficiencies, which may be related to prior

phosphatization (precursor converted to bone apatite). These results provide additional evidence for the expanding field of in vitro phosphatization.

In summary, a uniformly thin CO_3Ap formed on the surface of roughened Ti tightly based on this method. Moreover, CO_3Ap-Ti promotes the differentiation of pre-osteoblastic cells, osteogenesis, and osteointegration in the animal. Whether the other factor (i.e., crystallite size, coating amount) of CO_3Ap-Ti on made these benefits will be the subject for future studies. Nevertheless, as a bioactive implant application, CO_3Ap-Ti has tremendous beneficial potential for clinical use.

Bibliography

[1] X. Y. Liu, P. K. Chu, C. X. Ding, Surface modification of titanium, titanium alloys, and related materials for biomedical applications. *Mat Sci Eng R* 47, 49-121 (2004).

[2] C. Oldani, A. Dominguez. Titanium as a Biomaterial for Implants. Recent Advances in Arthroplasty. InTech; (2012).

[3] A. F. Mavrogenis, R. Dimitriou, J. Parvizi, G. C. Babis, Biology of implant osseointegration. *J Musculoskelet Neuronal Interact* 9, 61-71 (2009).

[4] P. I. Branemark, Osseointegration and its experimental background. *J Prosthet Dent* 50, 399-410 (1983).

[5] H. Hirai, A. Okumura, M. Goto, T. Katsuki, Histologic study of the bone adjacent to titanium bone screws used for mandibular fracture treatment. *J Oral Maxillofac Surg* 59, 531-537 (2001).

[6] T. Albrektsson, P. I. Branemark, H. A. Hansson, J. Lindstrom, Osseointegrated titanium implants. Requirements for ensuring a long-lasting, direct bone-to-implant anchorage in man. *Acta Orthop Scand* 52, 155-170 (1981).

[7] Y. T. Sul, C. B. Johansson, Y. Jeong, K. Roser, A. Wennerberg, T. Albrektsson, Oxidized implants and their influence on the bone response. *J Mater Sci Mater Med* 12, 1025-1031 (2001).

[8] S. Prasad, M. Ehrensberger, M. P. Gibson, H. Kim, E. A. Monaco, Biomaterial properties of titanium in dentistry. *J Oral Biosci* 57, 192-199 (2015).

[9] L. Zhang, Y. Ayukawa, R. Z. Legeros, S. Matsuya, K. Koyano, K. Ishikawa, Tissue-response to calcium-bonded titanium surface. *J Biomed Mater Res A* 95, 33-39 (2010).

[10] L. Jonasova, F. A. Muller, A. Helebrant, J. Strnad, P. Greil, Biomimetic apatite formation on chemically treated titanium. *Biomaterials* 25, 1187-1194 (2004).

[11] L. Le Guehennec, M. A. Lopez-Heredia, B. Enkel, P. Weiss, Y. Amouriq, P. Layrolle, Osteoblastic cell behaviour on different titanium implant surfaces. *Acta Biomater* 4, 535-543 (2008).

[12] Y. Tian, S. Y. Ding, H. Peng, et al, Osteoblast growth behavior on porous-structure titanium surface. *Appl Surf Sci* 261, 25-30 (2012).

[13] J. B. Nebe, L. Muller, F. Luthen, et al, Osteoblast response to biomimetically altered titanium surfaces. *Acta Biomater* 4, 1985-1995 (2008).

[14] J. M. Lee, J. I. Lee, Y. J. Lim, In vitro investigation of anodization and CaP deposited titanium surface using MG63 osteoblast-like cells. *Appl Surf Sci* 256, 3086-3092 (2010).

[15] R. Castellani, A. De Ruijter, H. Renggli, J. Jansen, Response of rat bone marrow cells to differently roughened titanium discs. *Clin Oral Implants Res* 10, 369-378 (1999).

[16] R. A. Gittens, T. Mclachlan, R. Olivares-Navarrete, et al, The effects of combined micron-/submicron-scale surface roughness and nanoscale features on cell proliferation and differentiation. *Biomaterials* 32, 3395-3403 (2011).

[17] X. Wen, X. Wang, N. Zhang, Microrough surface of metallic biomaterials: a literature review. *Biomed Mater Eng* 6, 173-189 (1996).

[18] J. Y. Park, C. H. Gemmell, J. E. Davies, Platelet interactions with titanium: modulation of platelet activity by surface topography. *Biomaterials* 22, 2671-2682 (2001).

[19] J. E. Davies, Mechanisms of endosseous integration. *Int J Prosthodont* 11, 391-401 (1998).

[20] R. Kriparamanan, P. Aswath, A. Zhou, L. Tang, K. T. Nguyen, Nanotopography: cellular responses to nanostructured materials. *J Nanosci Nanotechnol* 6, 1905-1919 (2006).

[21] G. L. Yang, F. M. He, X. F. Yang, X. X. Wang, S. F. Zhao, Bone responses to titanium implants surface-roughened by sandblasted and double etched treatments in a rabbit model. *Oral Surg Oral Med Oral Pathol Oral Radiol* 106, 516-524 (2008).

[22] S. A. Cho, K. T. Park, The removal torque of titanium screw inserted in rabbit tibia treated by dual acid etching. *Biomaterials* 24, 3611-3617 (2003).

[23] Y. Liu, Y. Zhou, T. Jiang, Y. D. Liang, Z. Zhang, Y. N. Wang, Evaluation of the osseointegration of dental implants coated with calcium carbonate: an animal study. *Int J Oral Sci* 9, 133-138 (2017).

[24] A. Kulkarni Aranya, S. Pushalkar, M. Zhao, R. Z. Legeros, Y. Zhang, D. Saxena, Antibacterial and bioactive coatings on titanium implant surfaces. *J Biomed Mater Res A* 105, 2218-2227 (2017).

[25] H. Takadama, T. Kokubo. In vitro evaluation of bone bioactivity. *Bioceramics and their clinical applications*. Elsevier; 2008:165-182.

[26] D. P. Rivero, J. Fox, A. K. Skipor, R. M. Urban, J. O. Galante, Calcium phosphate-coated porous titanium implants for enhanced skeletal fixation. *J Biomed Mater Res* 22, 191-201 (1988).

[27] H. Q. Nguyen, D. A. Deporter, R. M. Pilliar, N. Valiquette, R. Yakubovich, The effect of sol-gel-formed calcium phosphate coatings on bone ingrowth and osteoconductivity of porous-surfaced Ti alloy implants. *Biomaterials* 25, 865-876 (2004).

[28] J. Suwanprateeb, W. Suvannapruk, W. Chokevivat, S. Kiertkrittikhoon, N. Jaruwangsanti, P. Tienboon, Bioactivity of a sol-gel-derived hydroxyapatite coating on titanium implants in vitro and in vivo. *Asian Biomed (Res Rev News)* 12, 35-44 (2018).

[29] C. Liang, H. Wang, J. Yang, et al, Femtosecond laser-induced micropattern and Ca/P deposition on Ti implant surface and its acceleration on early osseointegration. *ACS Appl Mater Interfaces* 5, 8179-8186 (2013).

[30] J. H. Sörensen, L. Dürselen, K. Welch, et al, Biomimetic Hydroxyapatite Coated Titanium Screws Demonstrate Rapid Implant Stabilization and Safe Removal. *J Nanobiotechnology* 06, 20-35 (2015).

[31] V. S. Kattimani, S. Kondaka, K. P. Lingamaneni, Hydroxyapatite–-Past, Present, and Future in Bone Regeneration. *Bone and Tissue Regeneration Insights* 7, BTRI.S36138 (2016).

[32] J. O. Hollinger, J. Brekke, E. Gruskin, D. Lee, Role of bone substitutes. *Clin Orthop Relat Res* 324, 55-65 (1996).

[33] H. W. Yang, M. H. Lin, Y. Z. Xu, G. W. Shang, R. R. Wang, K. Chen, Osteogenesis of bone marrow mesenchymal stem cells on strontium-substituted nano-hydroxyapatite coated roughened titanium surfaces. *Int J Clin Exp Med* 8, 257-264 (2015).

[34] M. Nagano, T. Nakamura, T. Kokubo, M. Tanahashi, M. Ogawa, Differences of bone bonding ability and degradation behaviour in vivo between amorphous calcium phosphate and highly crystalline hydroxyapatite coating. *Biomaterials* 17, 1771-1777 (1996).

[35] K. Soballe, Hydroxyapatite ceramic coating for bone implant fixation. Mechanical and histological studies in dogs. *Acta Orthop Scand Suppl* 255, 1-58 (1993).

[36] G. M. Vidigal, Jr., L. C. Aragones, A. Campos, Jr., M. Groisman, Histomorphometric analyses of hydroxyapatite-coated and uncoated titanium dental implants in rabbit cortical bone. *Implant Dent* 8, 295-302 (1999).

[37] M. Weinlaender, E. B. Kenney, V. Lekovic, J. Beumer, 3rd, P. K. Moy, S. Lewis, Histomorphometry of bone apposition around three types of endosseous dental implants. *Int J Oral Maxillofac Implants* 7, 491-496 (1992).

[38] S. D. Cook, K. A. Thomas, J. F. Kay, M. Jarcho, Hydroxyapatite-coated titanium for orthopedic implant applications. *Clin Orthop Relat Res* 232, 225-243 (1988).

[39] F. Iamoni, G. Rasperini, P. Trisi, M. Simion, Histomorphometric analysis of a half hydroxyapatite-coated implant in humans: a pilot study. *Int J Oral Maxillofac Implants* 14, 729-735 (1999).

[40] Y. Y. Chung, S. C. Ki, K. Y. So, D. H. Kim, K. H. Park, Y. S. Lee, High revision rate of hydroxyapatite-coated ABG-I prosthesis. *J Orthop Sci* 14, 543-547 (2009).

[41] R. D. Bloebaum, J. A. Dupont, Osteolysis from a press-fit hydroxyapatite-coated implant. A case study. *J Arthroplasty* 8, 195-202 (1993).

[42] C. J. Oosterbos, H. Vogely, M. W. Nijhof, et al, Osseointegration of hydroxyapatite-coated and noncoated Ti6Al4V implants in the presence of local infection: a comparative histomorphometrical study in rabbits. *J Biomed Mater Res* 60, 339-347 (2002).

[43] S. L. Wheeler, Eight-year clinical retrospective study of titanium plasma-sprayed and hydroxyapatite-coated cylinder implants. *Int J Oral Maxillofac Implants* 11, 340-350 (1996).

[44] Z. Artzi, G. Carmeli, A. Kozlovsky, A distinguishable observation between survival and success rate outcome of hydroxyapatite-coated implants in 5-10 years in function. *Clin Oral Implants Res* 17, 85-93 (2006).

[45] R. Z. Legeros, Calcium phosphates in oral biology and medicine. *Monogr Oral Sci* 15, 1-201 (1991).

[46] K. Ishikawa, Carbonate apatite bone replacement: learn from the bone. *J Ceram Soc Jpn* 127, 595-601 (2019).

[47] K. Hayashi, R. Kishida, A. Tsuchiya, K. Ishikawa, Honeycomb blocks composed of carbonate apatite, beta-tricalcium phosphate, and hydroxyapatite for bone regeneration: effects of composition on biological responses. *Mater Today Bio* 4, 100031 (2019).

[48] K. Ishikawa, Y. Miyamoto, A. Tsuchiya, K. Hayashi, K. Tsuru, G. Ohe, Physical and Histological Comparison of Hydroxyapatite, Carbonate Apatite, and beta-Tricalcium Phosphate Bone Substitutes. *Materials (Basel)* 11, 1993 (2018).

[49] A. Ogose, T. Hotta, H. Kawashima, et al, Comparison of hydroxyapatite and beta tricalcium phosphate as bone substitutes after excision of bone tumors. *J Biomed Mater Res B Appl Biomater* 72, 94-101 (2005).

[50] S. Weiner, H. D. Wagner, THE MATERIAL BONE: Structure-Mechanical Function Relations. *Annual Review of Materials Science* 28, 271-298 (1998).

[51] Y. Doi, T. Koda, N. Wakamatsu, et al, Influence of carbonate on sintering of apatites. *J Dent Res* 72, 1279-1284 (1993).

[52] M. Maruta, S. Matsuya, S. Nakamura, K. Ishikawa, Fabrication of low-crystalline carbonate apatite foam bone replacement based on phase transformation of calcite foam. *Dent Mater J* 30, 14-20 (2011).

[53] K. Ishikawa, Bone Substitute Fabrication Based on Dissolution-Precipitation Reactions. *Materials* 3, 1138-1155 (2010).

[54] B. Xu, K. M. Poduska, Linking crystal structure with temperature-sensitive vibrational modes in calcium carbonate minerals. *Phys Chem Chem Phys* 16, 17634-17639 (2014).

[55] H. Madupalli, B. Pavan, M. M. J. Tecklenburg, Carbonate substitution in the mineral component of bone: Discriminating the structural changes, simultaneously imposed by carbonate in A and B sites of apatite. *J Solid State Chem* 255, 27-35 (2017).

[56] K. H. Stern, High Temperature Properties and Decomposition of Inorganic Salts Part 3, Nitrates and Nitrites. *J Phys Chem Ref Data* 1, 747-772 (1972).

[57] A. Prince. Phase diagrams of ternary gold alloys. APDIC; (1990).

[58] A. K. Kurella, M. Z. Hu, N. B. Dahotre, Effect of microstructural evolution on wettability of laser coated calcium phosphate on titanium alloy. *Materials Science & Engineering C-Biomimetic and Supramolecular Systems* 28, 1560-1564 (2008).

[59] K. Liu, L. Jiang, Metallic surfaces with special wettability. *Nanoscale* 3, 825-838 (2011).

[60] O. Albayrak, O. El-Atwani, S. Altintas, Hydroxyapatite coating on titanium substrate by electrophoretic deposition method: Effects of titanium dioxide inner layer on adhesion strength and hydroxyapatite decomposition. *Surf Coat Technol* 202, 2482-2487 (2008).

[61] B. Mavis, A. C. Taş, Dip Coating of Calcium Hydroxyapatite on Ti-6Al-4V Substrates. *J Am Ceram Soc* 83, 989-991 (2004).

[62] M. Wei, A. J. Ruys, M. V. Swain, S. H. Kim, B. K. Milthorpe, C. C. Sorrell, Interfacial bond strength of electrophoretically deposited hydroxyapatite coatings on metals. *J Mater Sci Mater Med* 10, 401-409 (1999).

[63] I. G. Beşkardeş, M. Gümüşderelioğlu, Biomimetic Apatite-coated PCL Scaffolds: Effect of Surface Nanotopography on Cellular Functions. *J Bioact Compat Polym* 24, 507-524 (2009).

[64] H. Zreiqat, S. M. Valenzuela, B. B. Nissan, et al, The effect of surface chemistry modification of titanium alloy on signalling pathways in human osteoblasts. *Biomaterials* 26, 7579-7586 (2005).

[65] L. Ponsonnet, V. Comte, A. Othmane, et al, Effect of surface topography and chemistry on adhesion, orientation and growth of fibroblasts on nickel-titanium substrates. *Mat Sci Eng C-Bio S* 21, 157-165 (2002).

[66] J. B. Lian, G. S. Stein, Concepts of osteoblast growth and differentiation: basis for modulation of bone cell development and tissue formation. *Crit Rev Oral Biol Med* 3, 269-305 (1992).

[67] N. Fratzl-Zelman, P. Fratzl, H. Horandner, et al, Matrix mineralization in MC3T3-E1 cell cultures initiated by beta-glycerophosphate pulse. *Bone* 23, 511-520 (1998).

[68] C. H. Chung, E. E. Golub, E. Forbes, T. Tokuoka, I. M. Shapiro, Mechanism of action of beta-glycerophosphate on bone cell mineralization. *Calcif Tissue Int* 51, 305-311 (1992).

[69] R. Shi, K. Hayashi, L. T. Bang, K. Ishikawa, Effects of surface roughening and calcite coating of titanium on cell growth and differentiation. *J Biomater Appl* 34, 917-927 (2020).

[70] D. Kabaso, E. Gongadze, S. Perutkova, et al, Mechanics and electrostatics of the interactions between osteoblasts and titanium surface. *Comput Methods Biomech Biomed Engin* 14, 469-482 (2011).

[71] C. H. Lohmann, L. F. Bonewald, M. A. Sisk, et al, Maturation state determines the response of osteogenic cells to surface roughness and 1,25-dihydroxyvitamin D3. *J Bone Miner Res* 15, 1169-1180 (2000).

[72] A. Wennerberg, T. Albrektsson, Effects of titanium surface topography on bone integration: a systematic review. *Clin Oral Implants Res* 20 Suppl 4, 172-184 (2009).

[73] G. Y. Jung, Y. J. Park, J. S. Han, Effects of HA released calcium ion on osteoblast differentiation. *J Mater Sci Mater Med* 21, 1649-1654 (2010).

[74] S. An, J. Ling, Y. Gao, Y. Xiao, Effects of varied ionic calcium and phosphate on the proliferation, osteogenic differentiation and mineralization of human periodontal ligament cells in vitro. *J Periodontal Res* 47, 374-382 (2012).

[75] S. Ma, Y. Yang, D. L. Carnes, et al, Effects of dissolved calcium and phosphorous on osteoblast responses. *J Oral Implantol* 31, 61-67 (2005).

[76] S. Raghavendra, M. C. Wood, T. D. Taylor, Early wound healing around endosseous implants: a review of the literature. *Int J Oral Maxillofac Implants* 20, 425-431 (2005).

Acknowledgments

I would first like to express my gratitude to Professor Kunio Ishikawa for his insightful advice and support in my whole doctoral life. He let me know what a real outstanding researcher should do.

I would also like to acknowledge Associate Professor Koichiro Hayashi for encouraging me to do better researches, giving me limitless suggestions and help. He never tires of teaching me how to analyze and correct mistakes in researches.

My thanks go out as well to Professor Kanji Tsuru of Fukuoka Dental College, Assistant Professor Akira Tsuchiya, Assistant Professor Ryo Kishida, Dr. Yuki Sugiura, and Dr. Melvin L. Munar who set examples for their students and me. They motivated me to be a better researcher and gave me a lot of perceptive advice and help in my experiments.

Likewise, I would like to thank my lovely colleagues in this laboratory. These persons are always smiling and full of passion that encouraged me to go through every bad situation, even small.

Finally, I extend my appreciation to the China Scholarship Council (CSC) for the financial support of my Ph.D. in Japan.